J Mater Sci: Mater Electron (2009) 20:99–104
DOI 10.1007/s10854-008-9624-2

# Growth of tin oxide rod-like and sheet-like structures

**Hyoun Woo Kim · Jong Woo Lee · Chongmu Lee**

Received: 18 July 2006 / Accepted: 31 January 2008 / Published online: 19 February 2008


**Abstract** We have obtained the rod-like and sheet-like structures of tin oxide ($SnO_2$) by carrying out the thermal evaporation of solid Sn powders with varying the $O_2$ partial pressure. We have employed X-ray diffraction, scanning electron microscope, transmission electron microscope and photoluminescence (PL) spectroscopy to characterize the as-synthesized product. Higher $O_2$ partial pressure in the synthesis process mainly gave rise to wider sheet-like structures, whereas lower $O_2$ partial pressure facilitated the growth of rod-like structures. The product was single crystalline rutile structure. PL spectra exhibited the visible light emission.

## 1 Introduction

Tin oxide ($SnO_2$) is an important metal oxide. As a transparent conducting oxide, it has a long history of use as an electronic conductor, primarily in the form of thin films. The material has received a great deal of attention due to its applications in optoelectronic devices including flat panel displays, solar energy cells [1] and so on.

Inorganic materials with different morphologies and size can exhibit different properties [2], even if they are made up of the same elements. Accordingly, various structural and morphological forms of $SnO_2$ materials have been fabricated over the past several years, including nanowires [3–6], nanoribbons or nanobelts [7–12], nanorods [13–15], nanotubes [16], nanodiskettes [17], and nanocomposites [18, 19].

Two-dimensional (2D) nanostructure such as nanosheet is also an important category of nanostructured materials, having large surface area exposed to the gaseous environment and being ideal objects for the fabrication of nanoscale devices which possess various interesting functions. Therefore, much attention has recently been paid to realization of 2D nanostructures; the nanosheets of various materials including Zn [20], Cd [21], ZnS [22], $Ga_2O_3$ [23], CuO [24], $Bi_2Se_3$ [25], $Ag_2S$ [26], and $Fe_7S_8$ [27] have been successfully fabricated. However, to the best of our knowledge, nearly no report on the synthesis of sheet-like structure of $SnO_2$ has been published. In this article, we found that an intentional control of oxygen in the processing gas could introduce a fascinating $SnO_2$ sheet-like structures. We have investigated the samples with respect to their structural and photoluminescence (PL) characteristics.

## 2 Experimental

Pure Sn powders were placed in an alumina boat, which was put in the middle of quartz tube inserted in a horizontal tube furnace. We used Si(001) as a starting material onto which a layer of chromium (Cr) was deposited. On top of the boat, a piece of the substrate was placed with the Cr-coated side downwards. The vertical distance between the alumina boat and the substrate was approximately 10 mm. During the experiment, the furnace was maintained at a temperature of 850 °C under a constant total gas pressure of 1 Torr for 2 h. Since our objective was to investigate the effect of the $O_2$ gas injection on the morphology of the $SnO_2$ nanostructures, the percentages of the $O_2$ and Ar partial pressure, respectively, were set to 3 and 97%, 4 and 96%, and 6 and 94%.

H. W. Kim (✉) · J. W. Lee · C. Lee
School of Materials Science and Engineering, Inha University, Incheon 402-751, Republic of Korea
e-mail: hwkim@inha.ac.kr

The synthetic process with a higher $O_2$ partial pressure (>10%) did not generate nanomaterials on the substrate. After evaporation, the substrate was cooled down and then removed from the furnace for analysis. A white layer was found on the surface of the substrate.

Glancing angle X-ray diffraction (XRD: CuK$\alpha_1$ radiation) patterns were obtained on a Philips X'pert MRD diffractometer with an incidence angle of 0.5°. Scanning electron microscopy (SEM) studies were carried out on a Hitachi S-4200. Further structural analysis using transmission electron microscopy (TEM) was performed on a Philips CM-200. For TEM observation, the products were ultrasonically dispersed in acetone, and then a drop of the suspension was placed on amorphous carbon films supported by copper grids and dried in air. PL spectrum was measured at room temperature by a 325 nm He–Cd laser (Kimon, 1K, Japan).

## 3 Results and discussion

Figure 1a, b shows typical side-view and plan-view SEM images of the product with the $O_2$ partial pressure of 3 and 4%, respectively, consisting of rod-like structures. The growth direction of the structures is randomized. Figure 1c shows typical side-view and plan-view SEM images of the product with the $O_2$ partial pressure of 6%. The product at 6% $O_2$ mainly consist of the structures which are close to wider sheets. Some sheet-like structures have average widths larger than 5 μm. The average diameter (width) distributions of the products are shown in Fig. 2. It is noteworthy that the maxima of average diameter distributions occur in range of 500–1,000 nm and 1,000–1,500 nm, respectively, for the samples grown at the $O_2$ partial pressures of 3 and 4%. Accordingly, statistical analysis indicates that the average width of produced $SnO_2$ structures increases with increasing the $O_2$ partial pressure in the range of 3–6%.

Figure 3a–c shows typical XRD patterns recorded from the products grown with the $O_2$ partial pressures of 3, 4, and 6%, respectively. The diffraction peaks of the (110), (101), (200), (211), (220), (002), (310), (112), (301), (202), (212), and (321) planes can be readily indexed to the tetragonal rutile structure of $SnO_2$ with lattice constants of $a = 4.738$ Å and $c = 3.187$ Å (JCPDS File No. 41-1445). No obvious reflection peaks from the impurities, such as unreacted Sn or other tin oxides, were detected. Since the peak positions of three XRD patterns are almost identical and the glancing-angle XRD pattern represents the structure of the products, we surmise that the products correspond to $SnO_2$ phase, regardless of $O_2$ partial pressure in the range of 3–6%.

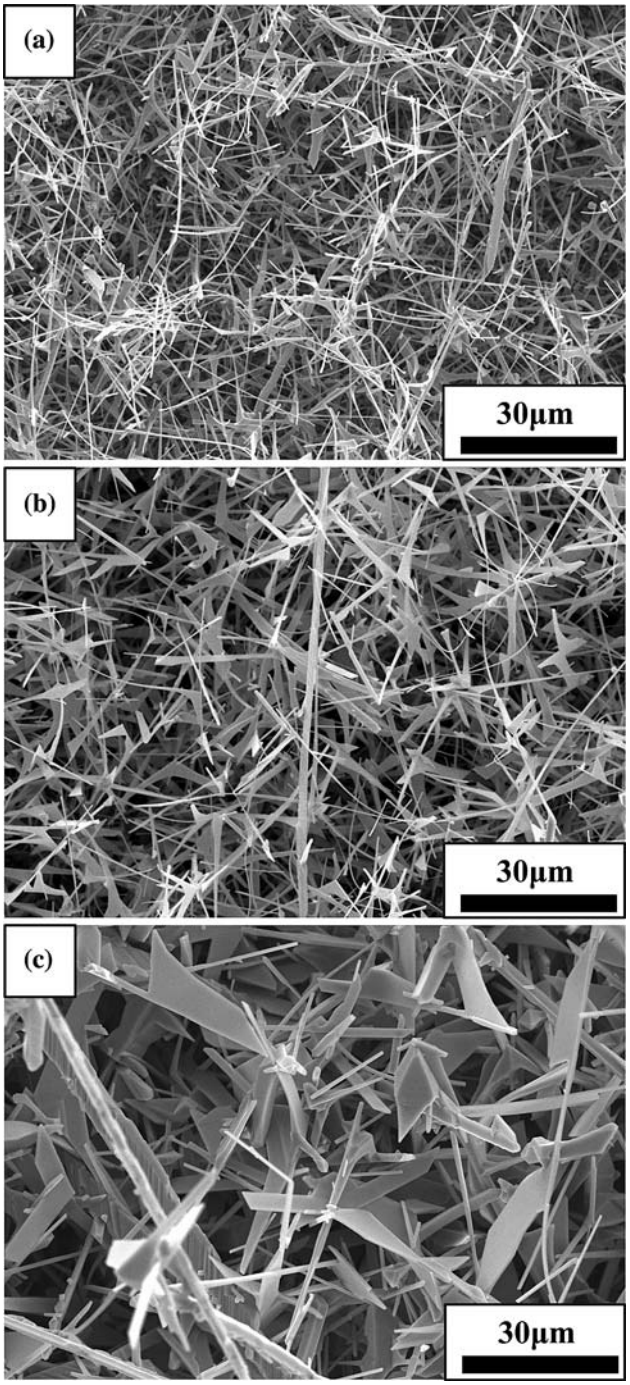


**Fig. 1** Plan-view SEM images of the products with the $O_2$ partial pressure of (**a**) 3%, (**b**) 4%, and (**c**) 6%

Low magnification TEM images of the product grown with an $O_2$ partial pressure of 6% are shown in Fig. 4a, b, indicating that small branches sprout from the sheet-like nanostructure. The associated selected area electron diffraction (SAED) pattern (Fig. 4c) taken from the nanosheets can be indexed as a tetragonal rutile $SnO_2$ single crystal, in good agreement with the XRD results presented above. Representative high resolution TEM

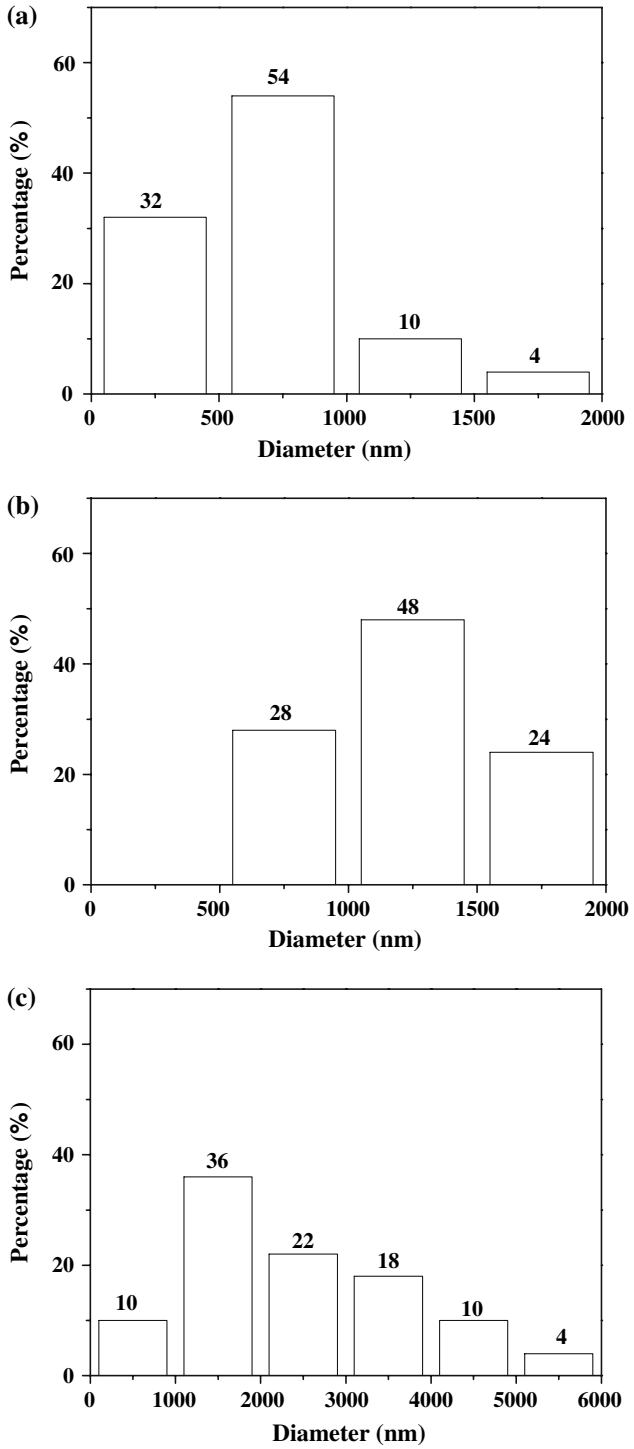


**Fig. 2** Average diameter (width) distributions of the products with the $O_2$ partial pressure of (**a**) 3%, (**b**) 4%, and (**c**) 6%

(HRTEM) image is given in Fig. 4d. Lattice fringes are clearly visible from the HRTEM image, revealing its single crystalline nature. The interplanar spacing is approximately 0.47 nm, corresponding to the (010) plane of tetragonal rutile $SnO_2$.

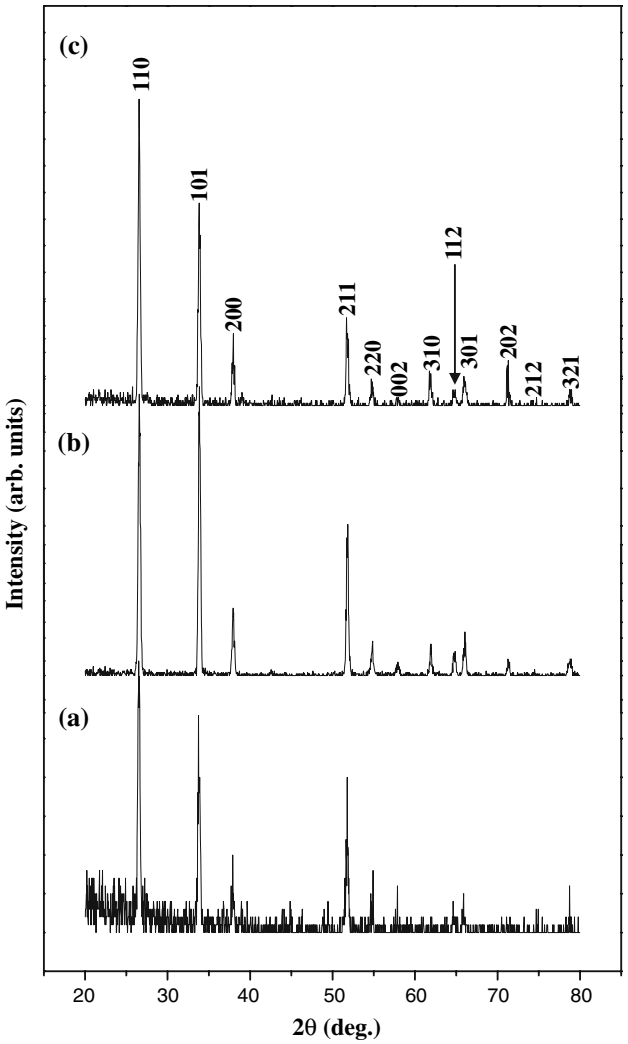


**Fig. 3** XRD patterns of the products with the $O_2$ partial pressure of (**a**) 3%, (**b**) 4%, and (**c**) 6%

We found that the $O_2$ content during the synthetic process played an important role in controlling the morphology (Figs. 1 and 2). When the $O_2$ content was increased to 6%, sheet-like 2D structures were dominantly obtained, while relatively greater amount of 1D nanostructures were produced with the $O_2$ content of 3%. There are two well-accepted mechanisms for the growth of 1D nanostructures, viz. the vapor–liquid–solid (VLS) and the vapor–solid (VS) mechanisms. In the present work, there was no evidence of metal-catalyst present on the tip of the structures from SEM analysis, regardless of $O_2$ content (Fig. 5). Therefore, the growth of the $SnO_2$ structure in the present route cannot be dominated by a VLS mechanism. This type of growth, which is close to a VS process, might be attributed to a diffusion-limited process in a supersaturated environment [28, 29]. The melting points of Sn and $SnO_2$, are approximately 232 and 1,630 °C, respectively. At a synthesis temperature of 850 °C in the present study,

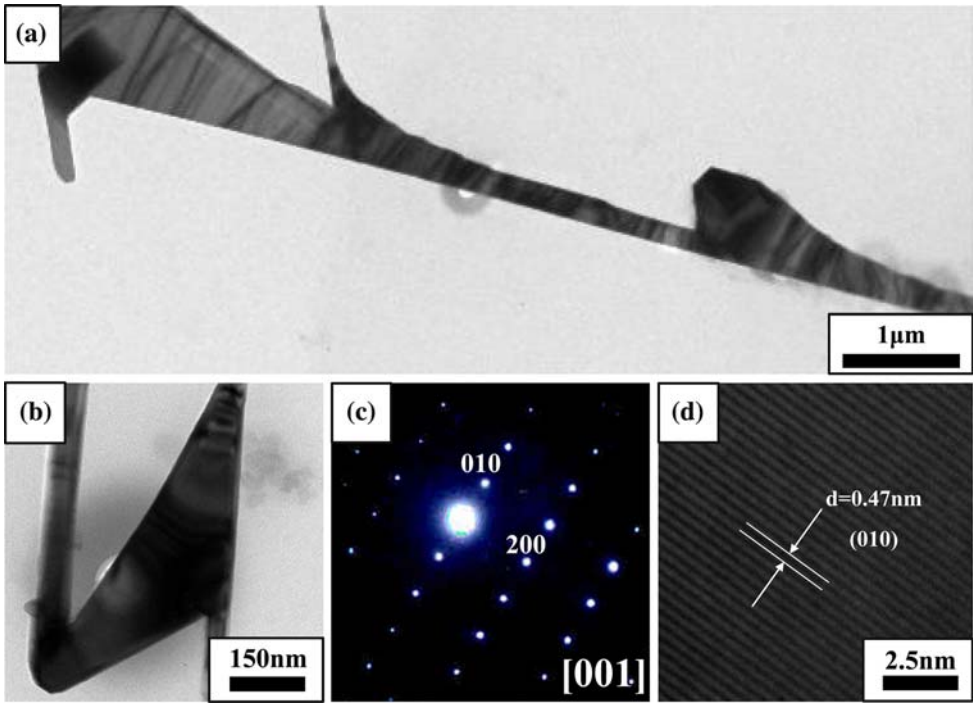


**Fig. 4** (**a**, **b**) Low magnification TEM images of product grown with the $O_2$ partial pressure of 6%. (**c**) SAED pattern of the [001] zone axis and (**d**) HRTEM image

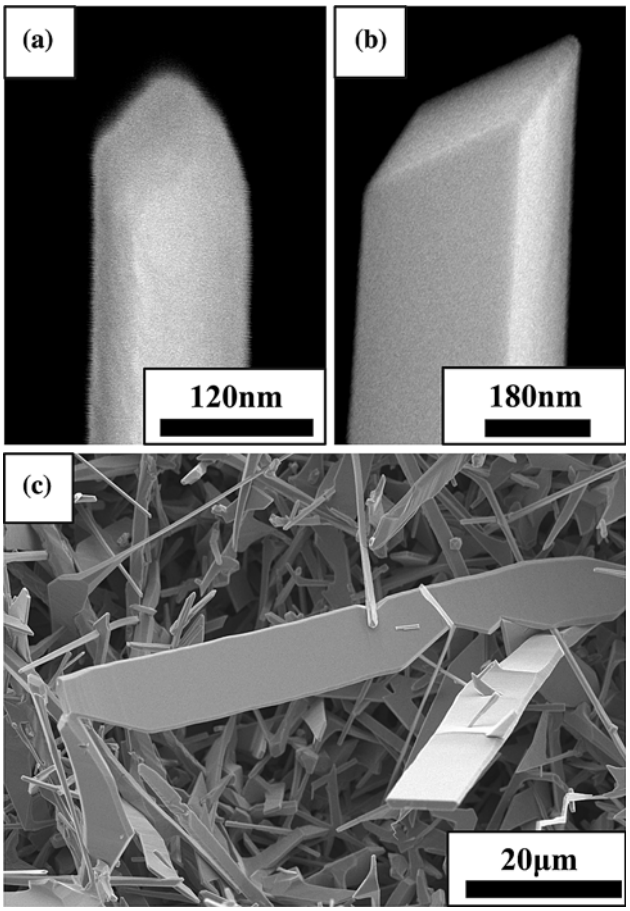


**Fig. 5** SEM images showing the end morphology of the typical product with the $O_2$ partial pressure of (**a**) 3%, (**b**) 4%, and (**c**) 6%

liquid Sn will oxidize rapidly in the presence of oxygen gas. It is generally agreed that the SnO forms at the initial stage of oxidation of Sn ($2Sn + O_2 \rightarrow 2SnO$) and that the SnO is metastable, spontaneously decomposing into liquid Sn and solid $SnO_2$ according to the reaction: $2SnO \rightarrow SnO_2 + Sn$ [29–31]. At the processing temperature, the SnO vapor can be transported to the substrate [32]. The higher oxygen partial pressure provides additional oxygen, which may facilitate a large supersaturation of $O_2$ gas, subsequently leading to a large supersaturation of SnO in its gaseous state and resulting in a fast condensation of solid $SnO_2$ on the substrate. Therefore, a large supersaturation may activate secondary growth sites and heterogeneous nucleation on the side of the 1D structures, tending to produce wider or sheet-like structures. Under small supersaturation, however, narrow 1D structures are easy to grow. This result is similar to that of a previous work reporting on the growth of $Ga_2O_3$, in which a small oxygen supersaturation facilitated the growth of 1D nanomaterials [33]. We surmise that the amount of oxygen in case of the process with an $O_2$ partial pressure of 6% is sufficient to provide the condition of oxygen supersaturation for the growth of $SnO_2$ sheets. Efforts are now in progress to pursue these routes in more detail to reveal the detailed synthesis mechanism. We have compared the amounts of products obtained via synthetic processes with various $O_2$ partial pressures. Figure 6a–c shows the film thicknesses of the deposited products with the $O_2$ partial pressure of 3, 4, and 6%, respectively, indicating that the average thickness increases with increasing the $O_2$ partial

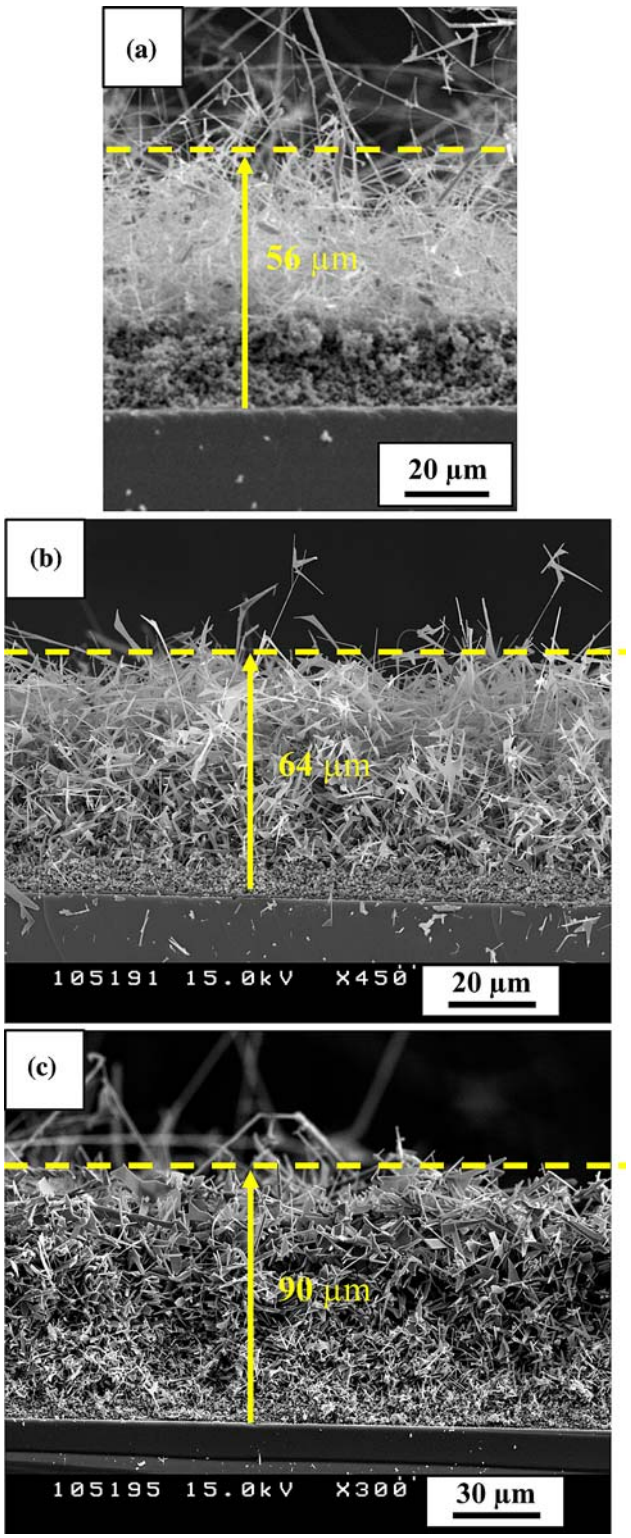


**Fig. 6** Side-view SEM images of the products with the $O_2$ partial pressure of (**a**) 3%, (**b**) 4%, and (**c**) 6%

pressure. Since the products were almost evenly coated on the whole surface of the substrate and the deposition time was set to 2 h for all three samples, we suggest that the yield of the products increases with increasing the $O_2$ partial pressure. We surmise that higher $O_2$ pressure generates a greater amount of SiO, ultimately contributing to the higher yield of the product.

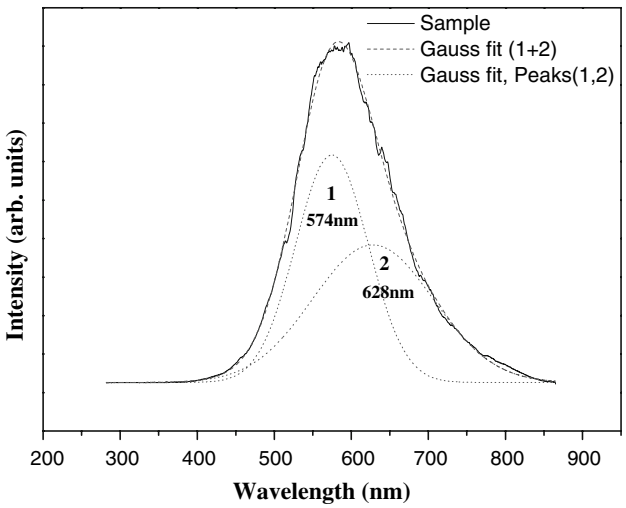


**Fig. 7** Room temperature PL spectrum with an excitation wavelength at 325 nm

Room-temperature PL spectrum of the product grown with the $O_2$ partial pressure of 6% was measured and shown in Fig. 7. There is an apparent broad, strong emission PL band, which can be a superimposition of several peaks. After multi-peak Gaussian fitting to all two major bands, we found that the Gaussian curves fit the original curves almost perfectly. The peak positions of the two Gaussian bands are located at about 574 and 628 nm, respectively. Therefore, the PL spectrum of the $SnO_2$ nanostructures mainly consists of two bands: a band which peaks at about 574 nm and another band which peaks at about 628 nm. Cheng et al. [34] and Maestre et al. [35] have previously reported the similar emissions peaked around 580 and 640 nm, respectively, from $SnO_2$ samples. The visible light emission is known to be related to defect levels within the band gap of $SnO_2$, associated with O vacancies or Sn interstitials that have formed during the synthesis process [34–37]. In the present study, high-temperature evaporation may generate various structural defects, contributing to the observed emissions. Further systematic study is necessary in order to reveal the mechanism of the observed emission.

## 4 Conclusions

In summary, we have performed a thermal evaporation of heating Sn powders under various $O_2$ partial pressures at 850 °C. The $O_2$ partial pressure determines the morphology of the final nanostructures, wide sheets being favored

by a high $O_2$ pressure. The results from XRD and HRTEM show that the product is single crystalline. We speculate about the mechanism by which $O_2$ content affects the morphology. The PL measurement with the Gaussian fitting show apparent visible light emission bands centered at 574 and 628 nm.

**Acknowledgement** This work was supported by the Inha Research Fund 2006.

## References

1. N. Amin, T. Isaka, A. Yamada, M. Konagai, Sol. Energy Mater. Sol. Cells **67**, 195 (2001)
2. J. Hulliger, Angew. Chem. Int. Ed. Engl. **33**, 143 (1994)
3. M. Zhang, G. Li, X. Zhang, S. Huang, Y. Lei, L. Zhang, Chem. Mater. **13**, 3859 (2001)
4. R.-Q. Zhang, Y. Lifshitz, S.-T. Lee, Adv. Mater. **15**, 635 (2003)
5. A. Kolmakov, Y. Zhang, G. Cheng, M. Moskovits, Adv. Mater. **15**, 997 (2003)
6. J.K. Jian, X.L. Chen, T. Xu, Y.P. Xu, L. Dai, M. He, Appl. Phys. A **75**, 695 (2002)
7. Z.R. Dai, Z.W. Pan, Z.L. Wang, Solid State Commun. **118**, 351 (2001)
8. Z.L. Wang, Z. Pan, Adv. Mater. **14**, 1029 (2002)
9. J.Q. Hu, X.L. Ma, N.G. Shang, Z.Y. Xie, N.B. Wong, C.S. Lee, S.T. Lee, J. Phys. Chem. B **106**, 3823 (2002)
10. X.S. Peng, L.D. Zhang, G.W. Meng, Y.T. Tian, Y. Lin, B.Y. Geng, S.H. Sun, J. Appl. Phys. **93**, 1760 (2003)
11. X.L. Ma, Y. Li, Y.L. Zhu, Chem. Phys. Lett. **376**, 794 (2003)
12. S.H. Sun, G.W. Meng, Y.W. Wang, T. Gao, M.G. Zhang, Y.T. Tian, X.S. Peng, L.D. Zhang, Appl. Phys. A **76**, 298 (2003)
13. Y. Liu, C. Zheng, W. Wang, C. Yin, G. Wang, Adv. Mater. **13**, 1883 (2001)
14. C. Xu, G. Xu, Y. Liu, X. Zhao, G. Wang, Scr. Mater. **46**, 789 (2002)
15. D.-F. Zhang, L.-D. Sun, J.-L. Yin, C.-H. Yan, Adv. Mater. **15**, 1022 (2003)
16. Z.R. Dai, J.L. Gole, J.D. Stout, Z.L. Wang, J. Phys. Chem. B **106**, 1274 (2002)
17. Z.R. Dai, Z.W. Pan, Z.L. Wang, J. Am. Chem. Soc. **124**, 8673 (2002)
18. J. Nemeth, I. Dekany, K. Süvegh, T. Marek, Z. Klencsar, A. Vertes, J.H. Fendler, Langmuir **19**, 3762 (2003)
19. W.-Q. Han, A. Zettle, Nano Lett. **3**, 681 (2003)
20. Y.C. Zhu, Y. Bando, Chem. Phys. Lett. **372**, 640 (2003)
21. J. Zhao, C. Ye, X. Fang, P. Yan, Z. Wang, L. Zhang, J. Cryst. Growth **277**, 445 (2005)
22. S.-H. Yu, J. Yang, Y.-T. Qian, M. Yoshimura, Chem. Phys. Lett. **361**, 362 (2002)
23. Z.R. Dai, Z.W. Pan, Z.L. Wang, J. Phys. Chem. B **106**, 902 (2002)
24. R. Yang, L. Gao, Solid State Commun. **134**, 729 (2005)
25. H. Cui, H. Liu, X. Li, J. Wang, F. Han, X. Zhang, R.I. Boughton, J. Solid State Chem. **177**, 4001 (2004)
26. M. Chan, L. Gao, Mater. Lett. **60**, 1059 (2006)
27. X.H. Kong, T.J. Lou, Y.D. Li, J. Alloys Compd. **390**, 236 (2005)
28. W.W. Mullins, R.F. Sekerka, J. Appl. Phys. **35**, 444 (2002)
29. J. Guojian, Z. Hanrui, Z. Jiang, R. Meiling, L. Wenlan, W. Fengying, Z. Baolin, J. Mater. Sci. **35**, 63 (2000)
30. D.-W. Yuan, R.-F. Yan, G. Simkovich, J. Mater. Sci. **34**, 2911 (1999)
31. J.C. Nover, F.D. Richardson, Trans. Inst. Min. Metall. **81**, 63 (1972)
32. J.Q. Hu, X.L. Ma, N.G. Shang, Z.Y. Xie, N.B. Wong, C.S. Lee, S.T. Lee, J. Phys. Chem. B **106**, 3823 (2002)
33. J.-S. Lee, K. Park, S. Nahm, S.-W. Kim, S. Kim, J. Cryst. Growth **244**, 287 (2002)
34. B. Cheng, J.M. Russell, W. Shi, L. Zhang, E.T. Samulski, J. Am. Chem. Soc. **126**, 5972 (2004)
35. D. Maestre, A. Cremades, J. Piqueras, J. Appl. Phys. **95**, 3027 (2004)
36. J. Hu, Y. Bando, Q. Liu, D. Goldberg, Adv. Funct. Mater. **13**, 493 (2003)
37. S.-S. Chang, D.K. Park, Mater. Sci. Eng. B **95**, 55 (2002)